

光学学报

不同偏置条件下CMOS图像传感器质子辐照损伤效应的实验与分析

聂栩¹, 王祖军^{1,2*}, 王百川², 薛院院², 黄港¹, 赖善坤¹, 唐宁¹, 王茂成², 赵铭彤², 杨馥羽², 王忠明²

¹湘潭大学材料科学与工程学院, 湖南 湘潭 411105;

²强脉冲辐射环境模拟与效应国家重点实验室(西北核技术研究所), 陕西 西安 710024

摘要 应用在空间辐射环境下的互补金属氧化物半导体图像传感器(CIS)会受到高能质子辐照损伤, 导致性能退化, 严重时甚至功能失效。为了分析CIS高能质子辐照损伤机理, 本文以0.18 μm工艺CIS为研究对象, 利用西安200 MeV质子应用装置开展了注量分别为 1×10^{10} 、 5×10^{10} 、 1×10^{11} p/cm²的100 MeV质子辐照实验。获得了单粒子瞬态响应的典型特征和暗信号、暗信号分布、暗信号尖峰及随机电码信号(RTS)等敏感参数的退化规律, 揭示了不同偏置条件和不同注量下CIS高能质子辐照损伤的物理机制。实验结果表明: 对暗信号而言, 加偏置条件比未加偏置条件变化显著; 质子辐照诱发的位移损伤和电离损伤引起暗信号的增大; 位移损伤诱发的体缺陷诱发暗信号尖峰的产生, 且随着辐照注量的增大而增多; 空间电荷区中不同类型的体缺陷导致两能级和多能级RTS的产生。

关键词 遥感与传感器; CMOS图像传感器; 质子辐照; 瞬态响应; 暗信号; 随机电码信号

中图分类号 TN386.5

文献标志码 A

DOI: 10.3788/AOS230592

1 引言

互补金属氧化物半导体图像传感器(CIS)是实现光电转换的半导体元器件。随着半导体工艺的进步, CIS性能得到了显著提升^[1], 因其低功耗、高集成度、较强的抗辐射能力等诸多优势日益凸显, 从而在星敏感器、天文观测及空间遥感等空间领域逐渐取代CCD图像传感器, 并且已在航天领域发挥重要作用。例如, 美国国家航空和宇宙航行局(NASA)发射的“火星2020”探测器上的23台相机中, 有10台采用了互补金属氧化物半导体(CMOS)图像传感器技术, 可提供详细的地形彩色图像, 以实现安全导航、硬件自检, 以及引导样本收集的解决方案^[2]。北京空间机电研究所研制的CMOS相机, 装载在微小卫星上, 主要任务和目的是对星箭分离状态、双星分离状态进行实时拍摄监视^[3]。

然而, 工作在空间辐射环境中的CIS会受到空间粒子辐射损伤的影响, 导致器件性能参数退化, 成像质量下降。CIS辐照损伤效应主要有: 位移损伤效应、单粒子效应和总剂量效应^[4-5]。目前国内外对CIS辐照损伤效应开展了大量研究。Goiffon等^[6-7]开展了不同能量中子和质子辐照实验, 提出了一种预测暗电流分布的模型, 分析了质子和中子诱导CIS暗电流非均匀

性和暗电流分布的相似性及损伤机理; 王祖军等^[8-14]开展了CIS的⁶⁰Co γ射线、X射线、电子、中子、质子等粒子辐照损伤效应的实验研究, 比较了不同能量、不同注量下暗信号、暗信号尖峰和随机电码信号(RTS)等辐射敏感参数的退化规律和损伤机理; 通过建立CMOS图像传感器的器件模型和不同注量中子辐照后位移损伤的缺陷模型, 获得电荷转移效率随中子辐照注量的变化关系, 分析了其随中子累积注量的变化规律^[15]。李豫东等^[16-17]对不同能量质子辐照CIS诱发暗电流、暗信号等性能参数退化规律以及物理机制作出了分析; 徐守龙等^[18-19]通过对CIS开展⁶⁰Co γ射线辐射实验研究, 获得了像素阵列各区域内响应信号的均匀性、暗电流等参数随辐照剂量的变化关系。然而, 国内外针对CIS的高能质子辐照损伤的研究开展较少, 尤其在偏压条件对器件损伤效应的研究方面鲜有报道, 且质子损伤物理机制比较复杂。

因此, 本文基于西安200 MeV质子应用装置(XiPAF), 以国产的0.18 μm工艺CIS为研究对象, 搭建了辐照效应在线测试系统, 分析了单粒子瞬态响应的典型特征, 获得了暗信号、暗信号分布、暗信号尖峰及RTS等各敏感参数的退化规律, 深入揭示了不同偏置条件下高能质子辐照诱导CIS敏感参数退化的损伤机制, 为CIS的抗辐照加固提供数据支撑。

收稿日期: 2023-02-23; 修回日期: 2023-03-27; 录用日期: 2023-04-17; 网络首发日期: 2023-05-08

基金项目: 国家自然科学基金(U2167208, 11875223)、国家重点实验室基金(SKLIPR1803, SKLIPR2012, SKLIPR2113)

通信作者: *wzj029@qq.com

2 实验样品和条件

2.1 实验样品

实验样品是 $0.18 \mu\text{m}$ 工艺的 CMOS 图像传感器，有效像素阵列由 2040×2048 个像素单元组成，像元尺寸为 $11 \mu\text{m} \times 11 \mu\text{m}$ ，采用 4T 像素结构，CIS 具有 12 位列并行模数转换器(ADC)，像素单元的所有信号通过 ADC 读出。图 1 为 4T PPD CIS 像素单元剖面图，主要包括空间电荷区(SCR)、浅槽隔离氧化层(STI)、阱位光电二极管(PPD)、传输管(M_{TG})、复位管(M_{RST})、行选择管(M_{SEL})、源跟随器(M_{SF})，以及浮置节点(FD)等区域。工作原理如下：首先 M_{RST} 对 FD 端进行复位，之后空间电荷区中的电荷在 M_{TG} 开启后传输到 FD 端，并在 FD 端中完成电荷到电压的转换，转换电压后， M_{SF} 用于放大 FD 的电压信号，最后 M_{SEL} 接通，输出放大的电压信号。

2.2 实验条件

辐照实验在XiPAF上进行,实验测试环境始终处于暗场下,选择能量为100 MeV的质子,注量分别为 1×10^{10} 、 5×10^{10} 、 1×10^{11} p/cm²。进行质子辐照时,一组样品加偏置电压,一组样品不加偏置电压;加偏置电压的样品被安装在辐照测试系统上,不加偏置电压的样品引脚悬空,辐照过程保证CIS处于暗场环境。现场可编程逻辑门阵列(FPGA)辐照测试系统主要提供CIS的驱动信号和串行外设接口(SPI)寄存器配置时序,并将采集到的图像数据传输到远程控制端,以此实现远程控制CIS进行图像采集并完成数据的实时传输与分析。

3 实验结果与分析

3.1 质子诱导的单粒子瞬态响应

质子诱导产生的单粒子瞬态响应主要表现为瞬态

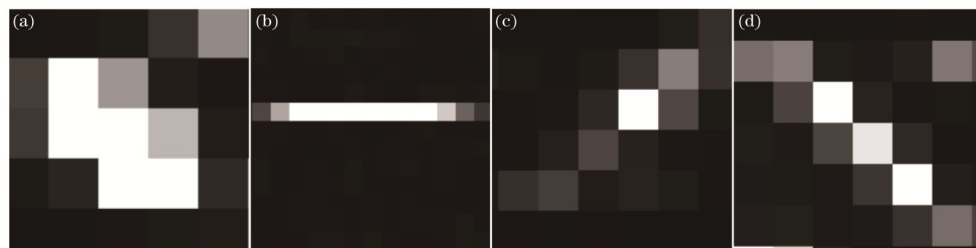


图2 质子辐照诱发的瞬态亮斑和亮线。(a) 瞬态亮斑;(b)、(c)、(d)瞬态亮线

Fig. 2 Transient bright spot and lines induced by proton irradiation. (a) Transient bright spot; (b), (c), (d) transient bright lines

3.2 暗信号

在无光注入又无其他方式注入信号电荷的条件下,CIS的输出信号为暗信号,输出电流为暗电流,是空间环境中CIS的辐射敏感参数。暗信号和暗电流密切相关。根据欧洲标准EMVA1288可知,平均暗信号和暗电流的转化关系^[21]为

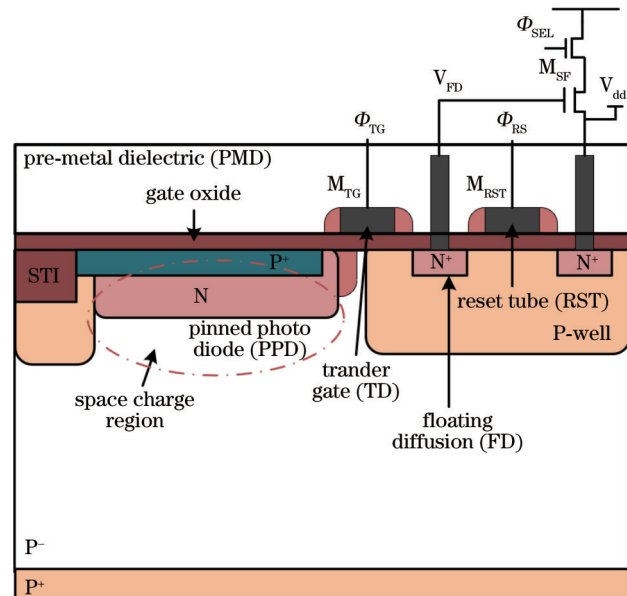


图1 4T PPD CMOS图像传感器像素单元剖面图^[20]

Fig. 1 Section view of pixel unit in 4T PPD type CMOS image sensor^[20]

亮斑和亮线，从辐照后暗图像中提取 $170 \text{ pixel} \times 170 \text{ pixel}$ 的子图像进行研究。图 2 所示为质子诱发的不同形态的单粒子瞬态亮斑和亮线，产生这些现象的原因，主要是由于高能质子与硅材料晶格原子发生弹性核反应、非弹性核碰撞反应，产生次级重离子，次级重离子在材料中沉积能量，在质子运行轨迹上会电离出大量的电子-空穴对，如图 3 所示为粒子入射轨迹。这些电子-空穴对不仅会被收集到像素单元的空间电荷区，还会被收集到单个或相邻几个像素单元中。当被收集到单个像素中时，瞬态电离电荷会导致暗信号尖峰的产生；被收集到几个相邻像素中时，会形成亮斑或一条亮线。这些单粒子瞬态亮斑和亮线不会永久存在，辐照后会立即消失。

$$\mu_y = \mu_{y,\text{dark}} + I_d t_{\text{exp}}, \quad (1)$$

式中: $\mu_{y, \text{dark}}$ 是积分时间为零时无光照条件下的平均暗信号; I_d 为暗电流; t_{exp} 为积分时间; μ_y 为当积分时间为 t_{exp} 时在无光照条件下的平均暗信号, 可以看出, 暗信号的退化规律与暗电流一致。因此, 可结合暗电流的退化机理分析暗信号的退化机理。图 4 所示为质子辐

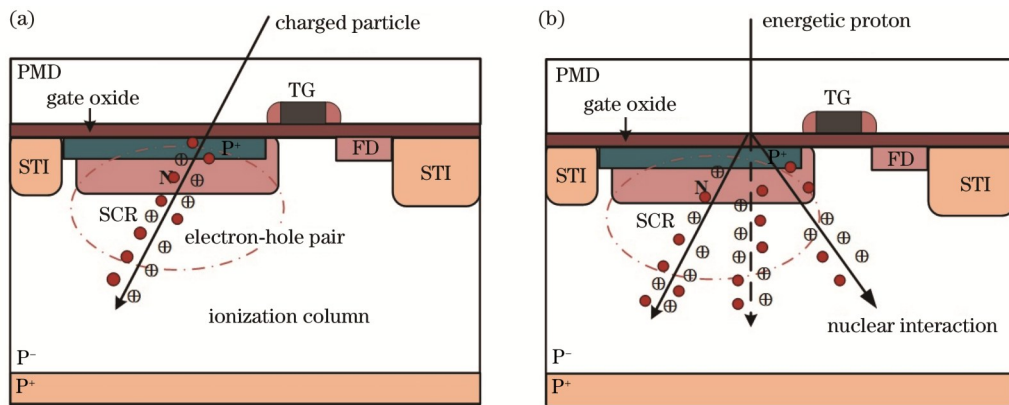


图3 粒子入射轨迹。(a)重离子入射轨迹;(b)质子入射轨迹

Fig 3 Particle incident trajectory. (a) Charged particle incident trajectory; (b) proton incident trajectory

照诱发 CIS 暗电流的产生机制图。从图 4 可以看到, CIS 暗电流主要包括体暗电流、表面暗电流和扩散暗电流。体暗电流的产生区域主要集中在 SCR 中, 表面暗电流主要存在于 STI 与 PPD 接触面和 PPD 与传输栅(TG) 交叠区域; 扩散暗电流主要存在于 SCR 周围。

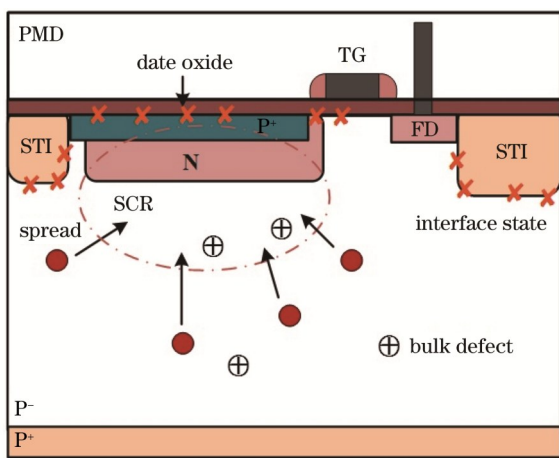


图4 CIS暗电流的产生机制图

Fig 4 Generation mechanism of CIS dark current

体暗电流主要是由于质子辐照诱发 CIS 产生体缺陷, 这些体缺陷会在 SCR 中产生新的产生-复合中心, 促进电子-空穴对的形成。导致体暗电流的增大。在 SCR 中, 电子-空穴对应该满足以下关系: $np \ll n_i^2$, 产生-复合的净产生率为^[22]为

$$U(E_t) = \frac{\sigma_n \sigma_p V_{th} N_t n_i}{\sigma_n \exp\left(\frac{E_t - E_i}{kT}\right) + \sigma_p \exp\left(\frac{E_i - E_t}{kT}\right)}, \quad (2)$$

式中: σ_n, σ_p 分别为电子和空穴俘获截面; V_{th} 为载流子热运动速率; E_i 为本征费米能级; N_t 为单位体积内缺陷密度; p 和 n 分别为空穴浓度和电子浓度; n_i 为本征载流子浓度; E_t 为缺陷能级; k 为玻尔兹曼常数; T 为绝对温度。净产生率与温度、缺陷能级、电子和空穴浓度的俘获截面有关。当缺陷能级处于禁带中央, 即 $E_t = E_i$,

时, 载流子的净产生率达到最大值, 其值为

$$U = \frac{\sigma_n \sigma_p V_{th} N_t n_i}{\sigma_n + \sigma_p}。 \quad (3)$$

SCR 的载流子寿命为

$$\tau_0 = \tau_n + \tau_p = \frac{1}{\sigma_n V_{th} N_t} + \frac{1}{\sigma_p V_{th} N_t} = \frac{\sigma_n + \sigma_p}{\sigma_n \sigma_p V_{th} N_t}, \quad (4)$$

式中, τ_n 和 τ_p 分别为电子和空穴的载流子寿命。则体暗电流密度为

$$J_{\text{generation}} = \int_0^W q U(E_t) dx \approx \frac{q n_i W}{\tau_0} = \frac{q n_i W \sigma_n \sigma_p V_{th}}{\sigma_n + \sigma_p} N_t, \quad (5)$$

式中: $J_{\text{generation}}$ 为体暗电流密度; W 为耗尽区宽度。因此, 体暗电流密度与单位体积内缺陷密度成正比。

表面暗电流由于电离损伤诱发界面态电荷的存在, 在接触面形成表面暗电流。在 Si-SiO₂ 界面处, 产生-复合的净产生率为^[22]为

$$U(E_{it}) = \frac{\sigma_n \sigma_p V_{th} D_{it}(E_{it})}{\sigma_n \exp\left(\frac{E_{it} - E_i}{kT}\right) + \sigma_p \exp\left(\frac{E_i - E_{it}}{kT}\right)}, \quad (6)$$

式中: E_{it} 为界面态缺陷能级; $D_{it}(E_{it})$ 为界面态密度。则表面暗电流密度为

$$J_{\text{surface}} = \int_{E_v}^{E_c} q U(E_{it}) d(E_{it}) = \frac{q n_i}{2} (\sigma_n \sigma_p)^{1/2} V_{th} \pi k T D_{it}, \quad (7)$$

式中: E_v 为价带能级; E_c 为导带能级。由此可得, 表面暗电流与界面态缺陷成正比。在一定条件下, 界面态缺陷与辐照剂量 T_{ID} 成线性关系^[22]:

$$D_{it} \approx \frac{1}{2} N_{siH} \sigma_{it} N_{DH} \sigma_{DH} g_0 f_y x_H^2 T_{ID}, \quad (8)$$

式中: N_{siH} 为 Si-H 键密度; σ_{it} 为 Si-H 键密度对质子的俘获截面; σ_{DH} 为含氢缺陷对质子的俘获截面; N_{DH} 为含氢缺陷密度; g_0 为电子-空穴对产生率; f_y 为空穴产额; x_H 为漂移长度; T_{ID} 为辐照总剂量。由此可得, 在一定条件下, 表面暗电流与辐射剂量成正比。

质子辐照 CIS 会产生电离损伤和位移损伤。电离损伤使表面暗电流密度增大; 位移损伤使体暗电流密

度增大。与表面暗电流和体暗电流相比,扩散暗电流密度可忽略不计。因此,质子辐照CIS后,CIS暗电流密度可表示为

$$J_{\text{dark}} = J_{\text{generation}} + J_{\text{surface}} = \frac{qn_i W \sigma_n \sigma_p V_{\text{th}}}{\sigma_n + \sigma_p} N_t + \frac{qn_i}{2} (\sigma_n \sigma_p)^{1/2} V_{\text{th}} \pi k T D_{\text{it}} \quad (9)$$

根据暗电流和暗信号的转化关系可以得出,质子辐照损伤产生的暗信号主要包括两部分:一部分是由位移损伤产生的暗信号;另一部分为电离损伤产生的暗信号。随着质子辐照注量的增大,缺陷密度相对增大,导致暗信号增大。

从辐照后的暗图像中提取200 pixel×200 pixel的子图像进行研究,图5表示不同注量对CIS输出图像的影响,辐照前,输出图像为黑图,不存在暗信号尖峰,辐照后暗信号尖峰显著增加,并且随着辐照注量的增大而增多,当质子注量达到 $1 \times 10^{11} \text{ p/cm}^2$ 时,CIS内受

质子影响的像元数最多,图像质量明显下降。与单粒子瞬态响应形成的暗信号尖峰相比,这些暗信号尖峰始终存在且位置固定。

图6表示相同积分时间下,加偏压与不加偏压时,暗信号随辐照注量的变化曲线,其中DN是数字计数单位,是描述图像灰度值的常用计数单位(以下同)。可以看出,在不同的偏置条件下,平均暗信号增加的趋势是不同的。CIS暗信号在加偏置条件下比不加偏置条件下增加近50%。随辐照注量的增加,CIS暗信号也逐渐增大。满足式(9)。此外,加偏置电压下器件的暗信号较未加偏置电压下变化显著,这是由于像素单元内的N型金属氧化物半导体(NMOS)管对加偏压比较敏感,高能质子与NMOS相互作用诱发电离效应,产生大量的电子-空穴对,在电场的作用下,大量的电子向NMOS管的栅极移动,空穴则被Si-SiO₂界面处的缺陷和杂质捕获形成氧化层陷阱电荷,导致暗信号比不加偏压下变化更加显著。

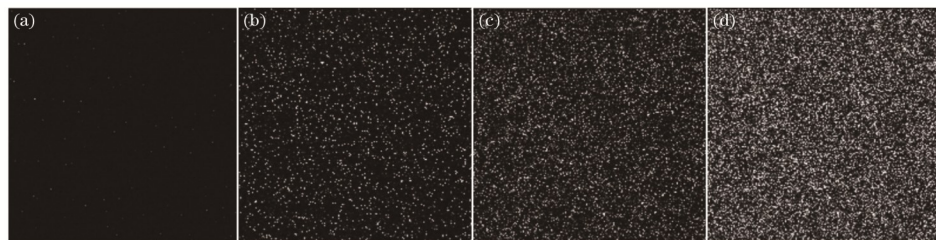


图5 加偏置电压(5 V)下不同辐照注量的暗信号输出图像。(a)辐照前;(b)质子注量为 $1 \times 10^{10} \text{ p/cm}^2$;(c)质子注量为 $5 \times 10^{10} \text{ p/cm}^2$;(d)质子注量为 $1 \times 10^{11} \text{ p/cm}^2$

Fig. 5 Dark signal output images under different radiation fluences with bias voltage of 5 V. (a) Before irradiation; (b) proton fluence is $1 \times 10^{10} \text{ p/cm}^2$; (c) proton fluence is $5 \times 10^{10} \text{ p/cm}^2$; (d) proton fluence is $1 \times 10^{11} \text{ p/cm}^2$

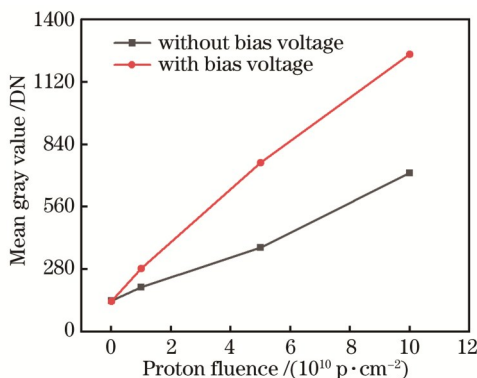


图6 加偏压与不加偏压时暗信号与质子辐照注量的关系
Fig. 6 Relationship between dark signal and proton radiation fluence with and without bias voltage

图7表示不同辐照注量下,暗信号随积分时间变化的关系曲线。质子辐照前,平均暗信号变化不明显;辐照后,CIS像素单元受损严重,且当积分时间较小时,CIS平均暗信号随积分时间的增大而近似呈线性增大;但当积分时间较大时,平均暗信号随积分时间的增大趋势减小,最后趋于饱和。主要是由于质子能量

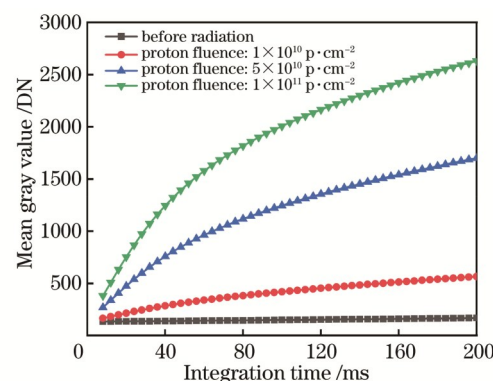


图7 暗信号与质子辐照注量的关系
Fig. 7 Curve of dark signal varying with proton irradiation fluence

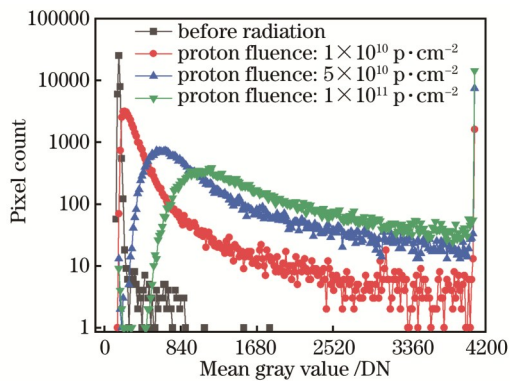


图8 不同质子辐照注量下对应暗信号的像素单元数分布图
Fig. 8 Distribution of pixel counts of dark signal under different proton radiation fluences

图8表示在不同质子注量下,对应暗信号值的像素单元数分布图,由于在CIS芯片生产过程中会引入少量的缺陷,CIS像素单元之间存在差异,因此,质子辐照前,暗信号呈高斯分布,产生少量的暗信号尖峰;辐照后,质子辐照诱发的电离损伤使暗信号在像素单元中呈高斯分布,质子诱发的位移损伤使暗信号呈 γ 分布,因此质子辐照诱发的暗信号分布曲线是由高斯

分布曲线和 γ 分布曲线卷积获得。随着辐照注量的增大,出现“拖尾”现象,这说明在高辐照注量下,产生暗信号尖峰的像元数目增加。暗信号高斯分布曲线右移主要是随着剂量增加,之前受辐照影响较小的像素单元暗信号进一步增加,导致器件像素单元整体暗信号增大。

3.3 暗信号尖峰

暗信号尖峰是位移损伤的典型特征现象,通常指在SCR产生的比平均暗信号至少大3倍的信号^[23]。高能质子与CIS晶格之间的弹性和非弹性碰撞,使晶格原子移位产生体缺陷,而这些体缺陷会充当载流子产生复合中心,导致暗信号尖峰的产生,在黑图上表现为大量的白斑和亮点,且在短期内不会消失。如图9所示,辐照前,由于芯片生产工艺带来的缺陷,存在少量的暗信号尖峰;随着辐照注量的增加,位移损伤剂量 D_d 增大,导致暗信号尖峰的数量和幅度不断增加。辐照注量达到 $1 \times 10^{10} \text{ p/cm}^2$ 时,部分像素单元暗信号显著增加,出现了图8中的“拖尾”现象。之后,随着辐照注量继续增加至 $1 \times 10^{11} \text{ p/cm}^2$ 时,输出暗信号整体上升,但没有出现明显的暗信号尖峰,出现图8中暗信号分布曲线右移的实验现象。

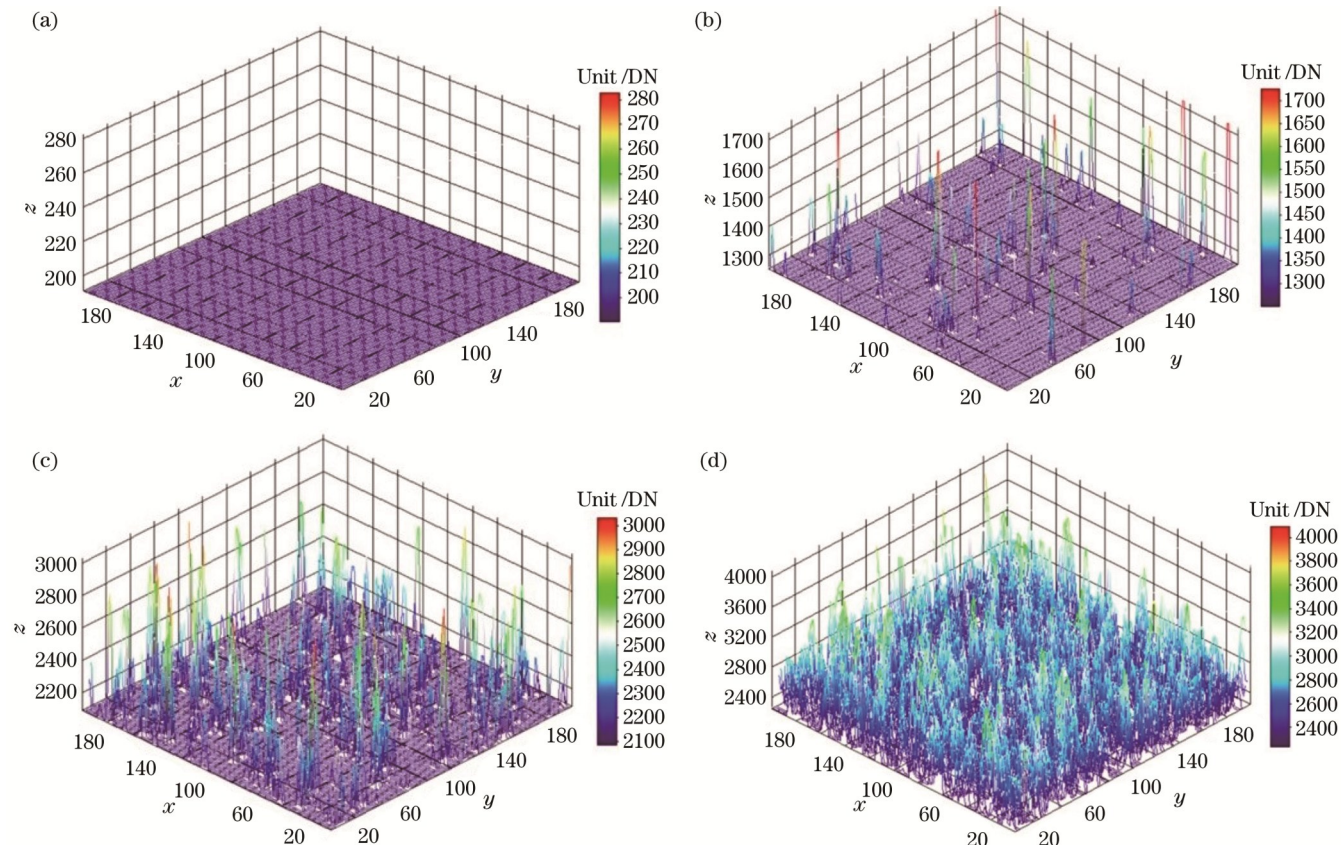


图9 质子辐照前后暗信号尖峰三维分布图。(a)辐照前;(b)质子注量为 $1 \times 10^{10} \text{ p/cm}^2$;(c)质子注量为 $5 \times 10^{10} \text{ p/cm}^2$;(d)质子注量为 $1 \times 10^{11} \text{ p/cm}^2$

Fig. 9 3D distributions of dark signal spike before and after proton radiation. (a) Before radiation; (b) proton fluence is $1 \times 10^{10} \text{ p/cm}^2$; (c) proton fluence is $5 \times 10^{10} \text{ p/cm}^2$; (d) proton fluence is $1 \times 10^{11} \text{ p/cm}^2$

3.4 RTS

RTS 是暗信号在两个或多个能级之间切换的现象。CIS 中的 RTS 表示像素中暗信号随时间的波动，这种现象在黑图上表现为一系列闪烁的像素点。随着像元尺寸逐渐缩小，源跟随器的面积也在不断缩小，导致 $1/f$ 低频噪声逐渐退化为 RTS，影响 CIS 的成像质量^[24]。RTS 主要源于质子在 CIS 图像传感器中产生的位移损伤，因此 RTS 与 CIS 晶格中缺陷的密度和分布密切相关。不同的点缺陷或缺陷簇形成缺陷能级是不同的，这导致 RTS 在两个或多个能级波动^[25]。图 10 表示由质子辐照诱发的 CIS 中典型两能级 RTS，以及所选像素中暗信号的平均值和标准变化。以像素单元 (1566, 117) 为例，其 RTS 变化幅度小、有序且平均值低，远小于像素单元 (1200, 1056) 和 (1566, 33)。这是因为各像素单元因位移损伤产生体缺陷的密度存在差异，导致其产生复合中心对载流子寿命的影响有着很大区别，最终表现各像素单元中两能级 RTS 有着明显差异。此外，图 11 表示质子辐照诱发的 CIS 像素点内的典型多能级 RTS 现象，与两能级 RTS 不同的是，多能级 RTS 因为产生缺陷种类较为复杂，其缺陷能级除了产生复合作用外还夹杂着捕获载流子作用，从而导致一定数目载流子的滞留，性能上表现为图 11 中信号变化曲线幅度较大且不规律，随着缺陷密度增加，变化更加明显，从像素单元 (137, 1000) 可以看出。

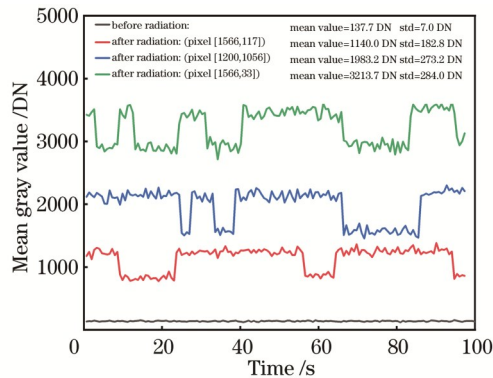


图 10 质子辐照诱发 CIS 典型的两能级缺陷

Fig. 10 Typical two-level defects in CIS induced by proton radiation

4 结 论

本文通过在 XiPAF 上开展 100 MeV 高能质子辐照实验，得到了质子辐照诱发 CIS 单粒子瞬态响应典型特征及敏感参数退化的实验规律。结果表明：单粒子瞬态响应的典型特征主要是一系列瞬态亮斑和亮线，由高能质子在运行轨迹上产生的电子-空穴对被几个像素单元收集而形成；质子诱发的累积效应（电离效应和位移效应）导致暗信号的增大，且随辐照注量的增大而增大；在相同质子注量下，暗信号在加偏置条件下比不加偏置条件下增加近 50%，主要是因为质子辐照

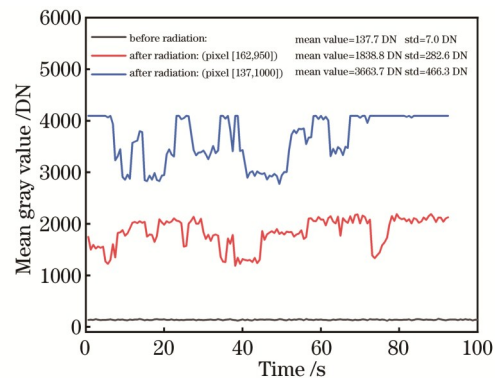


图 11 质子辐照诱发 CIS 典型的多能级缺陷

Fig. 11 Typical multi-level defects in CIS induced by proton radiation

诱发电离效应，在 CIS 像素单元内产生大量的电子-空穴对，在电场的作用下，大量的电子向 NMOS 管的栅极移动，空穴则被 Si-SiO₂界面处的缺陷和杂质捕获形成氧化物陷阱电荷；暗信号尖峰是位移损伤的典型特征，且随着辐照注量的增大而增大；质子辐射引起的两能级和多能级 RTS 与 SCR 中的体缺陷有关。本文实验有助于设计人员了解 CIS 的辐射损伤情况，并通过辐射加固设计提高其抗辐射能力。下一步将开展更多高能质子辐照实验，进一步研究 CIS 中的单粒子瞬态响应和敏感参数的退化机理。

参 考 文 献

- [1] 马精格 . CCD 与 CMOS 图像传感器的现状及发展趋势 [J]. 电子技术与软件工程, 2017(13): 103.
Ma J G. Current situation and development trend of CCD and CMOS image sensors[J]. Electronic Technology & Software Engineering, 2017(13): 103.
- [2] NASA Science. The camera on the mars 2020 mission perseverance rover [EB/OL]. (2020-06-25) [2022-11-11]. <https://mars.nasa.gov/mars2020/spacecraft/rover/cameras/>.
- [3] 王军, 李国宏 . CMOS 图像传感器在航天遥感中的应用 [J]. 航天返回与遥感, 2008, 29(2): 42-47.
Wang J, Li G H. The application of CMOS image sensor in space remote sensing[J]. Spacecraft Recovery & Remote Sensing, 2008, 29(2): 42-47.
- [4] 王祖军, 刘静, 薛院院, 等 . CMOS 图像传感器总剂量辐照效应及加固技术研究进展 [J]. 半导体光电, 2017, 38(1): 1-7.
Wang Z J, Liu J, Xue Y Y, et al. Progress of total ionizing dose radiation effects and hardening technology of CMOS image sensors[J]. Semiconductor Optoelectronics, 2017, 38(1): 1-7.
- [5] 王祖军, 林东生, 刘敏波, 等 . CMOS 有源像素图像传感器的辐照损伤效应 [J]. 半导体光电, 2014, 35(6): 945-950, 982.
Wang Z J, Lin D S, Liu M B, et al. Radiation damage effects on the CMOS active pixel sensors[J]. Semiconductor Optoelectronics, 2014, 35(6): 945-950, 982.
- [6] Virmontois C, Goiffon V, Magnan P, et al. Similarities between proton and neutron induced dark current distribution in CMOS image sensors[J]. IEEE Transactions on Nuclear Science, 2012, 59(4): 927-936.
- [7] Virmontois C, Goiffon V, Magnan P, et al. Displacement damage effects due to neutron and proton irradiations on CMOS image sensors manufactured in deep submicron technology[J]. IEEE Transactions on Nuclear Science, 2010, 57(6): 3101-

3108.

- [8] 王祖军, 薛院院, 贾同轩, 等. 不同剂量率伽马射线辐照PPD CMOS图像传感器的瞬态效应实验研究[C]//中国核科学技术进展报告(第七卷), 2021年学术年会论文集第6册. 北京: 中国核学会, 2021, 7: 124-132.
Wang Z J, Xue Y Y, Jia T X, et al. The experimental research of transient effects in PPD CMOS image sensors irradiated by gamma rays at different dose rates[C]//Progress Report of Nuclear Science and Technology in China (Volume 7), Volume 6 of the 2021 Academic Annual Conference Proceedings. Beijing: Chinese Nuclear Society, 2021, 7: 124-132.
- [9] 王祖军, 薛院院, 马武英, 等. 电离总剂量效应诱发PPD CMOS图像传感器性能退化的实验研究[C]//中国核科学技术进展报告(第五卷), 2017年学术年会论文集第6册, 2017, 05: 376-384.
Wang Z J, Xue Y Y, Ma W Y, et al. The experimental research of the performance degradation in PPD CMOS image sensors induced by total ionizing dose radiation effects[C]//Progress Report of Nuclear Science and Technology in China (Volume 5), Volume 6 of the 2017 Academic Annual Conference Proceedings. Beijing: Chinese Nuclear Society, 2017, 5: 376-384.
- [10] Xue Y Y, Wang Z J, Chen W, et al. Proton radiation effects on dark signal distribution of PPD CMOS image sensors: both TID and DDD effects[J]. Sensors, 2017, 17(12): 2781.
- [11] Xue Y Y, Wang Z J, Liu M B, et al. Research on proton radiation effects on CMOS image sensors with experimental and particle transport simulation methods[J]. Science China Information Sciences, 2017, 60(12): 120402.
- [12] Wang Z J, Xue Y Y, Chen W, et al. Comparison of the dark signal degradation induced by Gamma ray, proton, and neutron radiation in pinned photodiode CMOS image sensors[J]. Science China Information Sciences, 2019, 62(6): 069403.
- [13] Wang Z J, Xue Y Y, Chen W, et al. Fixed pattern noise and temporal noise degradation induced by radiation effects in pinned photodiode CMOS image sensors[J]. IEEE Transactions on Nuclear Science, 2018, 65(6): 1264-1270.
- [14] Wang Z J, Xue Y Y, Chen W, et al. Single particle transient response and displacement damage in CMOS image sensors induced by high energy neutrons at Back-n in CSNS facility[J]. Nuclear Instruments and Methods in Physics Research Section A: Accelerators, Spectrometers, Detectors and Associated Equipment, 2019, 920: 68-72.
- [15] 杨鲲, 霍勇刚, 王祖军, 等. 位移损伤诱发CMOS图像传感器电荷转移损失退化的理论模拟研究[J]. 光学学报, 2022, 42(7): 0723002.
Yang X, Huo Y G, Wang Z J, et al. Theoretical simulation of charge transfer loss degradation of CMOS image sensor induced by displacement damage[J]. Acta Optica Sinica, 2022, 42(7): 0723002.
- [16] 蔡毓龙, 李豫东, 文林, 等. 0.18 μm CMOS有源像素图像传感器质子辐照效应[J]. 红外与激光工程, 2020, 49(7): 20190433.
Cai Y L, Li Y D, Wen L, et al. Radiation effects of 0.18 μm CMOS APS by proton irradiation[J]. Infrared and Laser Engineering, 2020, 49(7): 20190433.
- [17] 傅婧, 李豫东, 冯婕, 等. 8T CMOS图像传感器质子辐照效应研究[J]. 原子能科学技术, 2021, 55(12): 2128-2134.
Fu J, Li Y D, Feng J, et al. Degradation characteristic of proton irradiated 8T CMOS image sensor[J]. Atomic Energy Science and Technology, 2021, 55(12): 2128-2134.
- [18] 徐守龙, 林奎成, 韩永超, 等. CMOS APS摄像机的γ射线辐射损伤模式与损伤表征研究[J]. 光学学报, 2020, 40(15): 1523002.
Xu S L, Lin K C, Han Y C, et al. Study on γ-ray irradiation damage mode and characterization of CMOS APS camera[J]. Acta Optica Sinica, 2020, 40(15): 1523002.
- [19] 徐守龙, 邹树梁, 韩永超, 等. 固态图像传感器的电离辐射响应均匀性[J]. 光学学报, 2019, 39(7): 0728007.
Xu S L, Zou S L, Han Y C, et al. Ionizing radiation response uniformity of solid-state image sensors[J]. Acta Optica Sinica, 2019, 39(7): 0728007.
- [20] Cao Z X, Zhou Y F, Li Q L, et al. Design of prototype high speed CMOS image sensors[J]. Proceedings of SPIE, 2013, 8908: 89082G.
- [21] European Machine Vision Association. Standard for characterization of image sensors and cameras: EMVA Standard 1288, Release 3.1[EB/OL]. [2022-12-09]. <https://www.emva.org/wp-content/uploads/EMVA1288-General-4.0ReleaseCandidate.pdf>.
- [22] Hardy T D. Effects of radiation damage on scientific charge coupled devices[D]. Burnaby: Simon Fraser University, 1997.
- [23] 王祖军, 薛院院, 刘卧龙, 等. CMOS图像传感器西安200 MeV质子应用装置H⁺辐照效应实验研究[J]. 现代应用物理, 2021, 12(3): 126-130, 139.
Wang Z J, Xue Y Y, Liu W L, et al. H⁺ beams irradiation effect of CMOS image sensor at Xi'an 200 MeV proton application facility[J]. Modern Applied Physics, 2021, 12(3): 126-130, 139.
- [24] Wang X Y, Rao P R, Mierop A, et al. Random telegraph signal in CMOS image sensor pixels[C]//2006 International Electron Devices Meeting, December 11-13, 2006, San Francisco, CA, USA. New York: IEEE Press, 2007.
- [25] Karami M A, Carrara L, Niclass C, et al. RTS noise characterization in single-photon avalanche diodes[J]. IEEE Electron Device Letters, 2010, 31(7): 692-694.

Experiment and Analysis of Damage of CMOS Image Sensor Induced by Proton Irradiation with Different Bias Conditions

Nie Xu¹, Wang Zujun^{1,2*}, Wang Baichuan², Xue Yuanyuan², Huang Gang¹, Lai Shankun¹, Tang Ning¹, Wang Maocheng², Zhao Mingtong², Yang Fuyu², Wang Zhongming²

¹School of Materials Science and Engineering, Xiangtan University, Xiangtan 411105, Hunan, China;

²State Key Laboratory of Intense Pulsed Irradiation Simulation and Effect, Northwest Institute of Nuclear Technology, Xi'an 710024, Shaanxi, China

Abstract

Objective Complementary metal oxide semiconductor (CMOS) image sensor is a semiconductor component that converts optical signals into electrical ones. With the progress in semiconductor technology, the performance of the CMOS image sensor has been significantly improved. Due to its many advantages, such as low power consumption, high integration, and strong radiation resistance, the CMOS image sensor has gradually replaced CCD image sensors in space optical communication, star sensors, astronomical observation, and space remote sensing, and played an important role in aerospace. However, in the space radiation environment, the CMOS image sensor will be affected by the radiation damage of space particles, resulting in the degradation of device performance parameters and imaging quality. High-energy protons are the main reason for the degraded performance of the CMOS image sensor in space environments. Therefore, it is important to study the damage effect and damage mechanism induced by proton irradiation of the CMOS image sensor for improving the reliability of its application in space radiation environments.

Methods The proton irradiation experiments are carried out on Xi'an 200 MeV Proton Application Facility (XiPAF), which provides proton beams in the range of 0–200 MeV. It selects protons with 100 MeV energy and the fluences of 1×10^{10} , 5×10^{10} , and 1×10^{11} p/cm². During proton irradiation, the device is in biased and unbiased states. The irradiation process ensures that the CMOS image sensor is in a dark environment. The test sample is a 0.18 μm CMOS image sensor and the total number of effective pixels is 2040 × 2048 with a pixel size of 11 μm × 11 μm. It adopts a 4T pixel structure. In this study, the continuous gray images and dark signals collected by the radiation effect test system of the CMOS image sensor at different integration times are taken as the output signals, and the curve of the changing dark signal with the irradiation fluence is obtained. The data gray images are extracted and processed by image analysis software, and the change rules of the dark signal distribution, dark spikes, and random telegraph signal are obtained. The typical characteristics of CMOS image sensor single-particle transient response under bias voltage are obtained.

Results and Discussions In this study, the single-particle transient response images with different shapes under bias voltage are obtained by conducting 100 MeV high-energy proton irradiation experiments, the change rules of dark signals and dark signal spikes under different fluences, and the changes of dark signals with irradiation fluence under different bias conditions are also obtained. The secondary particles generated by the interaction of high-energy protons and lattice atoms ionize on the transmission path to produce electron hole pairs, and the transient ionized charges collected in several adjacent pixel units will form transient bright spots or bright lines (Fig. 2). Since the N-type metal oxide semiconductor (NMOS) in the pixel unit is sensitive to the bias voltage during irradiation, the interaction between high-energy protons and the CMOS image sensor generates a large number of oxide defect charges and interface state charges, leading to a more significant change in the dark signal than that without bias voltage (Fig. 6). The volume defects generated by the interaction between protons and silicon atoms cause increasing dark signals and dark signal spikes. The increase in irradiation fluence results in rising volume defects, dark signals, and dark signal spikes (Figs. 5, 7, and 9). As proton irradiation damage mainly includes ionization damage and displacement damage, the dark signal distribution curve induced by proton irradiation is obtained by convolution of the Gaussian distribution curve induced by ionization damage and the gamma distribution curve induced by displacement damage. With the continuous increase in irradiation dose, the number of affected pixel units rises and the dark signal distribution curve shifts to the right (Fig. 8). The CMOS image sensor under proton irradiation will induce the generation of two-level and multi-level RTS, which is related to the density and distribution of bulk defects in the space charge region (Figs. 10 and 11).

Conclusions The experiments of high energy proton irradiation with 100 MeV carried out on XiPAF are introduced and the experimental law of CMOS image sensor performance degradation induced by proton irradiation is analyzed in this study. The typical characteristics of single-particle transient responses are mainly a series of transient bright spots and

bright lines, which are formed by the electron-hole pairs generated by high-energy protons on the trajectory and are collected by several pixel units. Proton-induced cumulative effects (ionization effect and displacement effect) lead to increasing dark signals which rise with the growing irradiation dose. Under the same amount of proton injection, the dark signal increases by nearly 50% under the condition with bias voltage than that without bias voltage. This is mainly because of the ionization effect induced by proton irradiation, which leads to the generation of a large number of electron-hole pairs in the pixel unit of the CMOS image sensor. Under the action of the electric field, a large number of electrons move to the gate of the NMOS, and the holes are trapped by defects and impurities at the Si-SiO₂ interface to form an oxide trap charge. Dark signal spikes are typical features of displacement damage and increase with the rising irradiation fluence. Two-level and multi-level RTSs induced by proton radiation are associated with bulk defects in SCR. This experiment helps designers understand the radiation damage of the CMOS image sensor and improve its radiation resistance through radiation reinforcement design. More high-energy proton irradiation experiments will be carried out to further study the degradation mechanism of single-particle transient responses and sensitive parameters in the CMOS image sensor.

Key words remote sensing and sensors; CMOS image sensor; proton irradiation; transient response; dark signal; random telegraph signal